A STUDY ON MATERIAL WORKABILITY BY UPSETTING OF NON-AXISYMMETRIC SPECIMENS BY FLAT DIES

S. Alexandrov

A. Ishlinskii Institute for Problems in Mechanics
Russian Academy of Sciences
Moscow, Russia

Department of Mechanical Engineering and
Advanced Institute of Manufacturing with High-Tech Innovations
National Chung Cheng University
Chiayi, Taiwan

M. Vilotic *

Department of Mechanical Engineering and
Advanced Institute of Manufacturing with High-Tech Innovations
National Chung Cheng University
Chiayi, Taiwan

Faculty of Technical Sciences
University of Novi Sad
Novi Sad, Serbia

Y.-R. Jeng

Department of Mechanical Engineering and
Advanced Institute of Manufacturing with High-Tech Innovations
National Chung Cheng University
Chiayi, Taiwan

M. Plancak

Faculty of Technical Sciences
University of Novi Sad
Novi Sad, Serbia

ABSTRACT

Upsetting is a typical test for determining the workability diagram. In most cases axisymmetric samples are used for such tests. However, the shape of samples may have a significant effect on the ductile fracture initiation. Therefore, a greater variety of sample geometry should lead to a more accurate shape of the workability diagram. A difficulty here is that a theoretical treatment of samples in which three-dimensional flow occurs is more difficult and time consuming as compared to axisymmetric samples under axisymmetric loading. This difficulty can be overcome in the case of the ductile fracture criterion based on the workability diagram and the average value of the triaxiality factor. In particular, if fracture occurs at free surfaces then it is sufficient to determine experimentally in-surface strains after several stages of the upsetting process, up to the initiation of ductile fracture. After that, the corresponding point of the workability diagram can be found by means of a simple analytical procedure and numerical integration. This approach is used in the present paper to correct the workability diagram using non-axisymmetric upsetting of five different samples made of steel. Some previous results are combined with the new results to obtain the workability diagram over a wide range of the triaxiality factor.

Keywords: Upsetting, Ductile fracture, Experimental-analytical method.

* Corresponding author (markovil@uns.ac.rs)

DOI : 10.1017/jmech.2014.67
Copyright © 2014 The Society of Theoretical and Applied Mechanics, R.O.C.
https://doi.org/10.1017/jmech.2014.67 Published online by Cambridge University Press

1. INTRODUCTION

Empirical ductile fracture criteria are often used to predict the initiation of ductile fracture in metal forming processes. These fracture criteria usually involve stress invariants and path-dependent integrals. Since it is not easy to create uniform distributions of stress and strain in specimen at large strains, it is important to develop methods for assessing such criteria using specimens in which the distribution of stress and strain is not uniform. On the other hand, it is desirable to exclude using numerical simulation since this requires constitutive equations and, in most cases, a law of friction. One of the methods satisfying the aforementioned criteria has been developed in [1]. The fracture criterion adopted in this paper is based on the workability diagram proposed in [2]. According to the method [1] it is sufficient to measure in-surface strains to apply the fracture criterion at points of a traction free surface. This method has been successfully used to determine the shape of the workability diagram in [3-5]. In these works, axisymmetric upsetting processes have been used. On the other hand, the method is applicable to non-axisymmetric processes as well and using such processes can result in a more accurate shape of the workability diagram. In particular, some non-axisymmetric processes have been already successfully used in ductile fracture studied [6,7]. In the present paper, experimental data from five types of non-axisymmetric processes are combined with the method [1] to arrive at an accurate shape of the workability diagram for the steel C45.

2. DUCTILE FRACTURE CRITERION BASED ON THE WORKABILITY DIAGRAM

The workability diagram is expressed mathematically as

$$\varepsilon_{eq}^{f} = F(\beta) \tag{1}$$

where ε_{eq}^{f} is the equivalent strain to fracture, β is the triaxiality ratio defined by $\beta = \sigma/\sigma_{eq}$ where σ is the hydrostatic stress and σ_{eq} is the Mises equivalent stress. By definition

$$\sigma = \frac{\sigma_{ij}\,\delta_{ij}}{3}, \quad \sigma_{eq} = \sqrt{\frac{3}{2}(\sigma_{ij}-\sigma\delta_{ij})(\sigma_{ij}-\sigma\delta_{ij})} \tag{2}$$

where σ_{ij} are the physical components of the stress tensor in any orthogonal coordinate system and δ_{ij} is Kroneker's symbol. Also, the equivalent strain is defined by the equation

$$\frac{d\varepsilon_{eq}}{dt} = \xi_{eq} \tag{3}$$

where t is the time. The equivalent strain rate ξ_{eq} is expressed through the physical components of the strain rate tensor ξ_{ij} as

$$\xi_{eq} = \sqrt{\frac{2}{3}\xi_{ij}\,\xi_{ij}}\,. \tag{4}$$

By definition, Eq. (1) predicts the initiation of ductile fracture at a material particle if β is constant at this particle throughout the process of deformation. One of the widely used empirical ductile fracture criteria based on the workability diagram is

$$\varepsilon_{eq}^{f} = F(\beta_{av})\,. \tag{5}$$

The difference between Eqs. (1) and (5) is that the argument of the function F in Eq. (5) is the average value of the triaxiality factor defined by

$$\beta_{av} = \frac{1}{\varepsilon_{eq}}\int_0^{\varepsilon_{eq}} \beta(\chi)\,d\chi \tag{6}$$

where χ is a dummy variable of integration. Equation (5) is valid for any strain path. In general, in order to find the function F involved in Eq. (1) experimentally it is necessary to test the material at β = constant. It is however a very difficult task, especially because a large range of β – value should be covered. Therefore, experimental data are usually combined with numerical simulation to find the function F using the empirical fracture criterion in Eq. (5). To this end, however, it is necessary to specify constitutive equations and, in many cases, frictional boundary conditions. This results in a significant loss of accuracy in the interpretation of experimental ductile fracture data. An advantage of the empirical ductile fracture criterion (Eq. (5)) over many other empirical ductile fracture criteria is that it can be reduced to a relation between in-surface strains if the initiation of fracture occurs on a traction free surface. Since there are well documented techniques to measure in-surface strains, no numerical treatment of the problem is necessary. The measured values of strains automatically account for the effect of friction on the strain path at the site of ductile fracture initiation. In particular, the average value of the triaxiality factor is expressed through the in-surface principal logarithmic strains ε_1 and ε_2 as [1]

$$\beta_{av} = \frac{2}{\varepsilon_{eq}}(\varepsilon_1 + \varepsilon_2)\,. \tag{7}$$

Note that the values of ε_1 and ε_2 are needed at the instant of fracture initiation but the determination of the equivalent strain requires integration over the strain path. Equation (7) is valid on any traction free surface. However, in most cases it has been applied for axisymmetric processes. Using non-axisymmetric processes can improve the accuracy of the experimental determination of the function F.

3. EXPERIMENTAL PROCEDURE AND RESULTS

Five types of non-axisymmetric processes have been used in this study. The material of the specimens is the steel C45. The initial shape of specimens is shown in Fig. 1. Three nominally identical specimens of each type have been tested to fracture in upsetting. The surface of specimens was examined for cracks by the naked eye. This is a typical method in research on ductile fracture in metal forming (see, for example, [8,9]). To measure the in-surface principal strains at the site of fracture initiation, orthogonal grid lines were

https://doi.org/10.1017/jmech.2014.67 Published online by Cambridge University Press

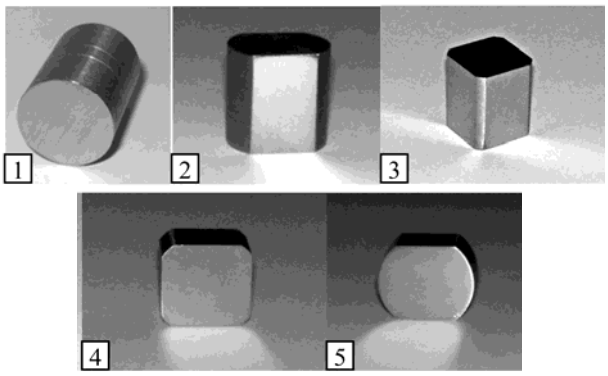


Fig. 1 Initial shape of specimens.

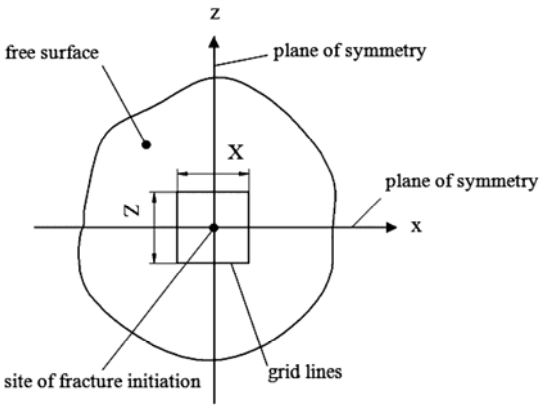


Fig. 2 Generic initial grid lines.

applied. Each process has at least two planes of symmetry. It is assumed that the initiation of fracture occurs at the intersection of these two planes and a free surface. This assumption is verified a posteriori. A generic site of fracture initiation is illustrated in Fig. 2. A Cartesian coordinate system (x, y, z) is chosen so that its origin is situated at the site of fracture initiation. The planes $x = 0$ and $z = 0$ coincide with the planes of symmetry. Then, the y-axis is orthogonal to the free surface. The initial grid lines are parallel to the x- and z- axes. The distance between these grid lines is denoted by Z in the z- direction and by X in the x- direction. At the initial instant, $X = Z = 3$mm. With no loss of generality, it is possible to assume that $\varepsilon_1 = \varepsilon_z$ and $\varepsilon_2 = \varepsilon_x$.

Specimens of type 1 are circular cylinders of initial diameter 18mm and initial height 18mm. The process is however non-axisymmetric (Fig. 3). The initiation of fracture occurred at the intersection of two planes of symmetry (point B in Fig. 3). The height of specimens of type 2 is 18mm. The other essential dimensions are shown in Fig. 4. The initiation of fracture occurred at the intersection of two planes of symmetry (point B or B' in Fig. 4). The height of specimens of type 3 is 18mm. The other essential dimensions are shown in Fig. 5. The initiation of fracture occurred at the intersection of two planes of symmetry (point B or B' or B'' or B''' in Fig. 5). The essential dimensions of specimens used in the process of types 4 and 5 are shown in Figs. 6 and 7, respectively. The initiation of fracture occurred at the intersection of two planes of symmetry (point B or B' in Figs. 6 and 7). In each case the direction of the two in-surface principal strains is evident. The measured values of Z and X are shown for three specimens of each type in Tables 1 to 5. The values in the lowest rows correspond to the maximum reduction at which no crack was detected. To illustrate the occurrence of cracks, one specimen of type 2 containing a crack is shown in Fig. 8.

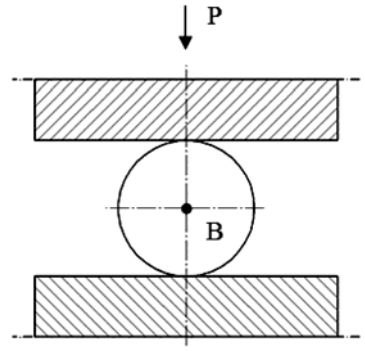


Fig. 3 Schematic diagram of the process (Type 1) and the site of fracture initiation (point B).

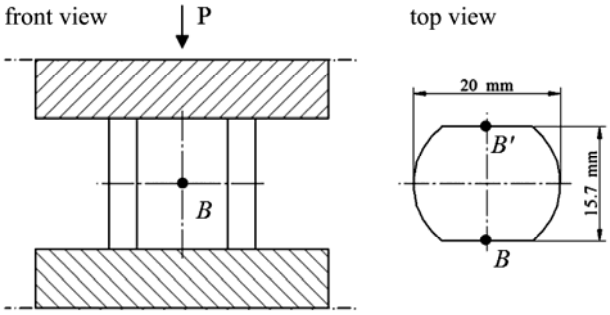


Fig. 4 Schematic diagram of the process (Type 2) and the site of fracture initiation (point B or B').

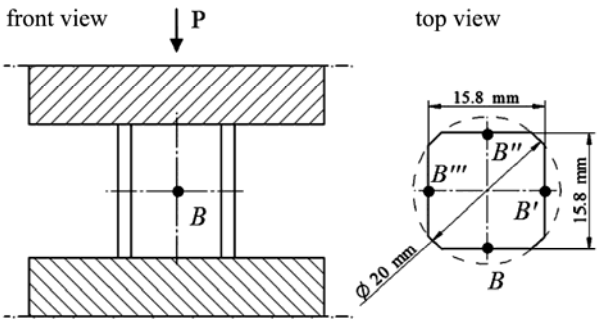


Fig. 5 Schematic diagram of the process (Type 3) and the site of fracture initiation (point B or B' or B'' or B''').

4. DETERMINATION OF THE FUNCTION F

The data presented in Tables 1 to 5 can be used to determine the equivalent strain to fracture. First, the discrete dependence of ε_x on ε_z is fitted to polynomials.

https://doi.org/10.1017/jmech.2014.67 Published online by Cambridge University Press

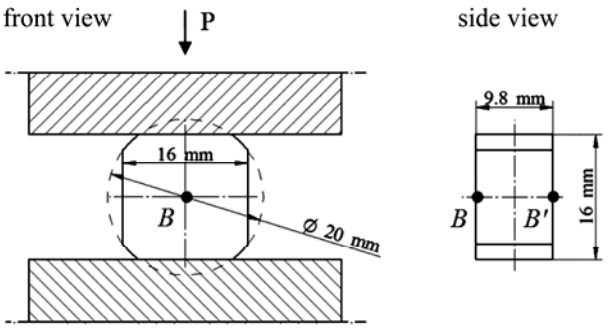


Fig. 6 Schematic diagram of the process (Type 4) and the site of fracture initiation (point B or B').

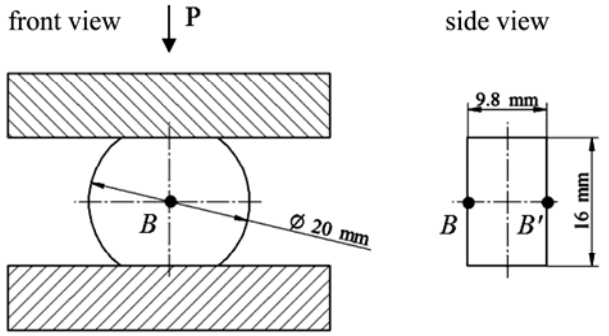


Fig. 7 Schematic diagram of the process (Type 5) and the site of fracture initiation (point B or B').

As a result, $\varepsilon_x = -0.37\varepsilon_z^2 - 1.31\varepsilon_z$ in the process of type 1, $\varepsilon_x = 0.59\varepsilon_z^2 - 0.42\varepsilon_z$ in the process of type 2, $\varepsilon_x = 0.46\varepsilon_z^2 - 0.47\varepsilon_z$ in the process of type 3, $\varepsilon_x = -0.81\varepsilon_z$ in the process of type 4, and $\varepsilon_x = 0.03\varepsilon_z^2 - 0.8\varepsilon_z$ in the process of type 5. In the Cartesian coordinates shown in Fig. 2 the equivalent strain rate at the site of fracture initiation is determined from (4) as

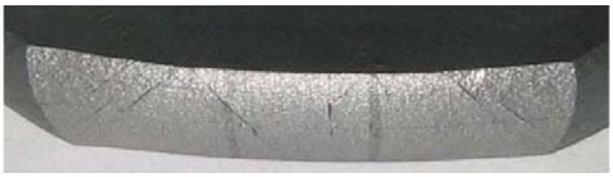


Fig. 8 Typical specimen of type 2 after testing.

$$\xi_{eq} = \sqrt{\frac{2}{3}(\xi_{xx}^2 + \xi_{yy}^2 + \xi_{zz}^2)}\,. \tag{8}$$

Elastic strains are neglected. Therefore, the normality rule associated with the von Mises yield criterion results in the equation of incompressibility. The latter is $\xi_{xx} + \xi_{yy} + \xi_{zz} = 0$ and Eq. (8) becomes

$$\xi_{eq} = \frac{2}{\sqrt{3}}\sqrt{\xi_{xx}^2 + \xi_{xx}\xi_{zz} + \xi_{zz}^2}\,. \tag{9}$$

In the case under consideration, the principal axes of the strain rate tensor remain fixed with respect to an element as it continues to deform. Therefore, $\xi_{xx} = \partial\varepsilon_x / \partial t$ and $\xi_{zz} = \partial\varepsilon_z / \partial t$. Then, substituting Eq. (9) into Eq. (3) and replacing differentiation with respect to t with differentiation with respect to ε_z yield

$$\varepsilon_{eq}^f = -\frac{2}{\sqrt{3}}\int_0^{\varepsilon_z^f}\sqrt{1 + \frac{d\varepsilon_x}{d\varepsilon_z} + \left(\frac{d\varepsilon_x}{d\varepsilon_z}\right)^2}\,d\varepsilon_z\,. \tag{10}$$

It has been taken into account here that $d\varepsilon_z / dt < 0$. The derivative involved in Eq. (10) is readily determined as a function of ε_z from the analytical expressions for ε_x given above. Therefore, the integral in this equation can be evaluated numerically. Then, using Eqs. (7), (10) and data from Tables 1 to 5 the value of β_{av} at fracture can be found with no difficulty. The final result is presented in Table 6. Using these values along with the results of standard tests [5,10] the function F can be approximated as

$$\varepsilon_{eq}^f = 0.8e^{-0.79\beta}\,. \tag{11}$$

This function and the experimental points obtained in the present study are illustrated in Fig. 9.

Table 1 Strains in the process of type 1.

Specimen 1				Specimen 2				Specimen 3			
Z [mm]	X [mm]	ε_z	ε_x	Z [mm]	X [mm]	ε_z	ε_x	Z [mm]	X [mm]	ε_z	ε_x
3.00	3.00	0.00	0.00	3.00	3.00	0.00	0.00	3.00	3.00	0.00	0.00
2.75	3.25	-0.09	0.08	2.73	3.20	-0.09	0.06	2.78	3.25	-0.08	0.08
2.58	3.48	-0.15	0.15	2.62	3.53	-0.14	0.16	2.63	3.49	-0.13	0.15
2.25	4.24	-0.29	0.35	2.26	4.35	-0.28	0.37	2.26	4.35	-0.28	0.37
1.98	5.07	-0.42	0.52	1.98	5.07	-0.42	0.52	1.99	5.08	-0.41	0.53
1.77	5.45	-0.53	0.60	1.83	5.51	-0.49	0.61	1.81	5.45	-0.51	0.60
1.65	5.72	-0.60	0.65	1.67	5.80	-0.59	0.66	1.66	5.69	-0.59	0.64
1.47	6.13	-0.71	0.71	1.51	6.17	-0.69	0.72	1.50	6.05	-0.69	0.70
1.34	6.50	-0.81	0.77	1.38	6.62	-0.78	0.79	1.37	6.51	-0.78	0.77
1.21	7.07	-0.91	0.86	1.27	7.12	-0.86	0.86	1.20	7.00	-0.92	0.85
1.13	7.52	-0.98	0.92	1.19	7.62	-0.92	0.93	1.11	7.62	-0.99	0.93
1.05	7.92	-1.05	0.97	1.10	8.13	ε_z^f =-1.00	ε_x^f =1.00	0.99	7.99	ε_z^f =-1.11	ε_x^f =0.98
1.00	8.32	-1.10	1.02								
0.95	8.86	ε_z^f =-1.15	ε_x^f =1.08								

https://doi.org/10.1017/jmech.2014.67 Published online by Cambridge University Press

Table 2 Strains in the process of type 2.

Specimen 1				Specimen 2				Specimen 3			
Z [mm]	X [mm]	ε_z	ε_x	Z [mm]	X [mm]	ε_z	ε_x	Z [mm]	X [mm]	ε_z	ε_x
3.00	3.00	0.00	0.00	3.00	3.00	0.00	0.00	3.00	3.00	0.00	0.00
2.66	3.24	-0.12	0.08	2.62	3.25	-0.14	0.08	2.65	3.27	-0.12	0.09
2.40	3.43	-0.22	0.13	2.43	3.41	-0.21	0.13	2.40	3.52	-0.22	0.16
2.16	3.74	-0.33	0.22	2.19	3.61	-0.31	0.19	2.22	3.67	-0.30	0.20
2.05	4.03	-0.38	0.30	2.00	3.78	-0.41	0.23	2.02	3.89	-0.40	0.26
1.84	4.17	-0.49	0.33	1.90	4.02	-0.46	0.29	1.87	4.12	-0.47	0.32
1.74	4.35	-0.54	0.37	1.73	4.28	-0.55	0.35	1.77	4.27	-0.53	0.35
1.67	4.56	-0.59	0.42	1.70	4.46	-0.57	0.40	1.72	4.48	-0.56	0.40
1.58	4.79	-0.64	0.47	1.66	4.71	-0.59	0.45	1.69	4.76	-0.57	0.46
1.52	4.94	-0.68	0.50	1.65	4.94	-0.60	0.50	1.59	4.94	-0.63	0.50
1.51	5.21	-0.69	0.55	1.60	5.08	-0.63	0.53	1.61	5.17	-0.62	0.54
1.48	5.39	-0.71	0.59	1.54	5.30	-0.67	0.57	1.57	5.40	-0.65	0.59
1.47	5.70	ε_z^f =-0.71	ε_x^f =0.64	1.52	5.49	ε_z^f =-0.68	ε_x^f =0.60	1.46	5.64	ε_z^f =-0.72	ε_x^f =0.63

Table 3 Strains in the process of type 3.

Specimen 1				Specimen 2				Specimen 3			
Z [mm]	X [mm]	ε_z	ε_x	Z [mm]	X [mm]	ε_z	ε_x	Z [mm]	X [mm]	ε_z	ε_x
3.00	3.00	0.00	0.00	3.00	3.00	0.00	0.00	3.00	3.00	0.00	0.00
2.70	3.23	-0.11	0.07	2.66	3.24	-0.12	0.08	2.64	3.21	-0.13	0.07
2.44	3.48	-0.21	0.15	2.40	3.47	-0.22	0.15	2.41	3.44	-0.22	0.14
2.21	3.69	-0.31	0.21	2.19	3.70	-0.31	0.21	2.14	3.68	-0.34	0.21
2.02	3.92	-0.40	0.27	1.95	3.86	-0.43	0.25	1.97	3.86	-0.42	0.25
1.90	4.16	-0.46	0.33	1.80	4.17	-0.51	0.33	1.85	4.12	-0.48	0.32
1.80	4.42	-0.51	0.39	1.71	4.36	-0.56	0.37	1.78	4.28	-0.52	0.35
1.70	4.57	-0.57	0.42	1.66	4.59	-0.59	0.43	1.71	4.51	-0.56	0.41
1.64	4.79	-0.60	0.47	1.61	4.80	-0.62	0.47	1.64	4.71	-0.60	0.45
1.60	5.01	-0.63	0.51	1.54	4.99	-0.67	0.51	1.55	4.93	-0.66	0.50
1.54	5.23	-0.67	0.56	1.49	5.30	-0.70	0.57	1.51	5.20	-0.69	0.55
1.46	5.51	-0.72	0.61	1.44	5.49	-0.73	0.60	1.43	5.32	-0.74	0.57
1.37	5.75	ε_z^f =-0.78	ε_x^f =0.65	1.41	5.76	ε_z^f =-0.76	ε_x^f =0.65	1.41	5.66	ε_z^f =-0.76	ε_x^f =0.63

Table 4 Strains in the process of type 4.

Specimen 1				Specimen 2				Specimen 3			
Z [mm]	X [mm]	ε_z	ε_x	Z [mm]	X [mm]	ε_z	ε_x	Z [mm]	X [mm]	ε_z	ε_x
3.00	3.00	0.00	0.00	3.00	3.00	0.00	0.00	3.00	3.00	0.00	0.00
2.40	3.59	-0.22	0.18	2.44	3.55	-0.21	0.17	2.42	3.55	-0.21	0.17
2.13	3.97	-0.34	0.28	2.15	3.98	-0.33	0.28	2.14	3.95	-0.34	0.27
2.01	4.15	-0.40	0.32	1.98	4.26	-0.42	0.35	2.01	4.20	-0.40	0.34
1.88	4.37	-0.47	0.38	1.86	4.33	-0.48	0.37	1.89	4.35	-0.46	0.37
1.75	4.53	-0.54	0.41	1.76	4.51	-0.53	0.41	1.82	4.55	-0.50	0.42
1.65	4.71	-0.60	0.45	1.64	4.75	-0.60	0.46	1.67	4.69	-0.59	0.45
1.59	4.95	-0.63	0.50	1.56	5.03	-0.65	0.52	1.59	5.01	-0.63	0.51
1.57	5.15	-0.65	0.54	1.51	5.24	-0.69	0.56	1.53	5.22	-0.67	0.55
1.53	5.32	-0.67	0.57	1.46	5.49	-0.72	0.60	1.47	5.44	-0.71	0.60
1.50	5.56	-0.69	0.62	1.38	5.53	-0.78	0.61	1.42	5.64	-0.75	0.63
1.42	5.74	-0.75	0.65	1.30	5.72	-0.84	0.65	1.33	5.94	-0.81	0.68
1.37	5.87	ε_z^f =-0.78	ε_x^f =0.67	1.19	5.92	ε_z^f =-0.92	ε_x^f =0.68	1.28	6.16	ε_z^f =-0.85	ε_x^f =0.72

https://doi.org/10.1017/jmech.2014.67 Published online by Cambridge University Press

Table 5 Strains in the process of type 5.

Specimen 1				Specimen 2				Specimen 3			
Z [mm]	X [mm]	ε_z	ε_x	Z [mm]	X [mm]	ε_z	ε_x	Z [mm]	X [mm]	ε_z	ε_x
3.00	3.00	0.00	0.00	3.00	3.00	0.00	0.00	3.00	3.00	0.00	0.00
2.43	3.60	-0.21	0.18	2.47	3.54	-0.19	0.17	2.45	3.56	-0.20	0.17
2.16	3.97	-0.33	0.28	2.20	3.96	-0.31	0.28	2.13	4.01	-0.34	0.29
2.00	4.21	-0.41	0.34	2.01	4.24	-0.40	0.35	1.93	4.21	-0.44	0.34
1.90	4.32	-0.46	0.36	1.93	4.33	-0.44	0.37	1.92	4.41	-0.45	0.38
1.84	4.48	-0.49	0.40	1.83	4.51	-0.49	0.41	1.76	4.47	-0.53	0.40
1.71	4.71	-0.56	0.45	1.70	4.69	-0.57	0.45	1.67	4.72	-0.59	0.45
1.61	4.85	-0.62	0.48	1.60	4.90	-0.63	0.49	1.55	4.88	-0.66	0.49
1.61	5.13	-0.62	0.54	1.55	5.11	-0.66	0.53	1.53	5.06	-0.67	0.52
1.51	5.24	-0.69	0.56	1.50	5.33	-0.69	0.57	1.48	5.21	-0.71	0.55
1.44	5.41	-0.73	0.59	1.48	5.41	-0.71	0.59	1.44	5.39	-0.73	0.59
1.36	5.65	-0.79	0.63	1.44	5.57	-0.73	0.62	1.39	5.54	-0.77	0.61
1.35	5.89	ε_z^f =-0.80	ε_x^f =0.68	1.40	6.29	ε_z^f =-0.76	ε_x^f =0.74	1.35	5.91	ε_z^f =-0.80	ε_x^f =0.68

Table 6 Values of ε_{eq}^f and β_{av}^f at fracture.

Type of process	ε_{eq}^f	β_{av}^f
1	1.17	–0.12
2	0.73	–0.29
3	0.82	–0.31
4	0.9	–0.34
5	0.87	–0.23

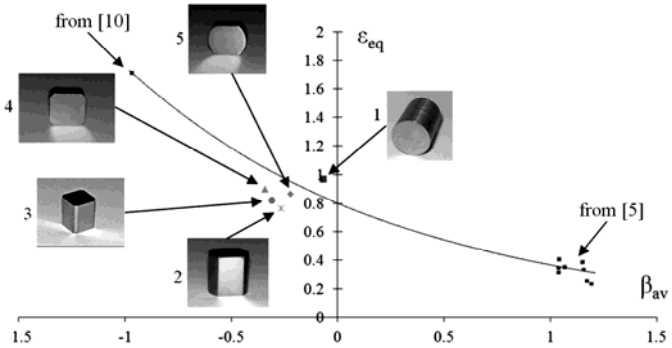


Fig. 9 Forming limit diagram of steel C45 (experimental data and their approximation by an exponential function).

5. CONCLUSIONS

Five non-axisymmetric tests to determine the workability diagram have been proposed and carried out. The initiation of fracture occurs in the vicinity of the intersection of two planes of symmetry and a traction free surface. This is advantageous for theoretical analysis of the state of strain at the site of fracture initiation since the principal strains differentiated with respect to the time are the principal strain rates. The purpose of this research has been to understand the effect of the shape of specimens on the values of ε_{eq} and β_{av} at fracture. It is seen from Fig. 9 that the experimental results for specimens of types 2, 3, 4, and 5 are located in a small range around $\beta_{av} = -0.25$. Therefore, it is sufficient to use just one of these tests to determine the corresponding value of ε_{eq} at fracture (one point of the workability diagram). On the other hand, β_{av} is rather close to zero in specimens of type 1. Therefore, this type of specimens can be used to replace the torsion test. The workability diagram for the steel C45 is represented by Eq. (11) in the range $-1 < \beta < 1.2$. The significance of the results obtained is that the forming limit diagram for the steel C45 has been approximated by Eq. (6) with a high accuracy.

ACKNOWLEDGMENTS

The research described was supported by grants RFBR-13-08-00969 (Russia) and TR035020 (Ministry of Science of Serbia).

REFERENCES

1. Vilotic, D., Plancak, M., Grbic, S., Alexandrov, S. and Chikanova, N., "An Approach to Determining the Workability Diagram Based on Upsetting Tests," *Fatigue & Fracture of Engineering Materials & Structures*, **26**, pp. 305–310 (2003).
2. Vujovic, V. and Shabaik, A., "Workability Criteria for Ductile Fracture," *Journal of Engineering Materials and Technology*, **108**, pp. 245–249 (1986).
3. Vilotic, D., Planchak, M., Chupkovich, D., Alexandrov, S. and Alexandrova, N., "Free Surface Fracture in Three Upsetting Tests," *Experimental Mechanics*, **46**, pp. 115–120 (2006).
4. Alexandrov, S. and Vilotic, D., "Theoretical Experimental Analysis of Fracture Initiation at the Free Surface in Upsetting Between Conical and Flat Dies," *Steel Research International*, **79**, pp. 375–381 (2008).
5. Alexandrov, S., Vilotic, D., Konjovic, Z. and Vilotic, M., "An Improved Experimental Method for Determining the Workability Diagram," *Experimental Mechanics*, **53**, pp. 699–711 (2013).
6. Sljapic, V., Hartley, P. and Pillinger, I., "Observations on Fracture in Axi-Symmetric and Three-Dimensional Cold Upsetting of Brass," *Journal of Materials Processing Technology*, **125-126**, pp.

https://doi.org/10.1017/jmech.2014.67 Published online by Cambridge University Press

267–274 (2002).
7. Lyamina, E., Alexandrov, S., Vilotic, D. and Movrin, D., "Effect of Shape of Samples on Ductile Fracture Initiation in Upsetting," *Steel Research International*, **81**, pp. 306–309 (2010).
8. El-Domiaty, A., "Cold-Workability Limits for Carbon and Alloy Steels," *Journal of Materials Engineering and Performance*, **8**, pp. 171–183 (1999).
9. Narayanasamy, R., Ramesh, T. and Pandey, K. S., "Workability Studies on Cold Upsetting of Al- Al_2O_3 Composite Material," *Materials & Design*, **27**, pp. 566–575 (2006).
10. Vilotić, D., Alexandrov, S., Plančak, M., Vilotić, M., Ivanišević, A. and Kačmarčik, I., "Material Formability at Upsetting by Cylindrical and Flat Dies," *Steel Research International*, pp. 1175–1178 (2012).

(Manuscript received May 31, 2013,
accepted for publication May 9, 2014.)

https://doi.org/10.1017/jmech.2014.67 Published online by Cambridge University Press